GEOLOGY | THE GEOLOGICAL SOCIETY OF AMERICA®

https://doi.org/10.1130/G47094.1

Manuscript received 11 October 2019
Revised manuscript received 9 January 2020
Manuscript accepted 28 January 2020

Published online 18 March 2020

Permeability of polydisperse magma foam

Jérémie Vasseur[1]*, Fabian B. Wadsworth[2] and Donald B. Dingwell[1]
[1]Department of Earth and Environmental Sciences, Ludwig-Maximilians-Universität, Theresienstrasse 41, 80333 Munich, Germany
[2]Department of Earth Sciences, Durham University, Durham DH1 4LY, UK

ABSTRACT

Effective models for the evolution of magma permeability are key to understanding shallow magma ascent and eruption dynamics. Models are generally empirical constructs, commonly focused on monodisperse systems, and unable to cope with the foam limit at high porosity. Here, we confirm that bubble size distributions in high-porosity pyroclasts are highly polydisperse. We combine collated experimental data and numerical simulations to test and validate a theoretically grounded percolation model for isotropic magma permeability, which accounts for the effect of polydispersivity of bubble sizes. We find that the polydispersivity controls the percolation threshold. It also serves as essential input into the scaling of permeability that is required to achieve universality in the description of permeability. Our model performs well against collated published data for the permeability of high-porosity volcanic rocks. We then extend this model to predict the viscous and inertial contributions to fluid flow that are required to model magma outgassing in all regimes. Our scaling relationship holds across the full range of porosity, from the percolation threshold to the open-foam limit.

INTRODUCTION

Permeability can exert a first-order control on the explosive potential of magmas rising through the crust (e.g., Mueller et al., 2008; Degruyter et al., 2012; Cassidy et al., 2018). Yet models for magma permeability remain empirical, semi-empirical, or limited to specific systems (Klug and Cashman, 1996; Saar and Manga, 1999; Mueller et al., 2008; Farquharson et al., 2015; Gonnermann et al., 2017). These models are typically calibrated against data sets collected for natural or experimental volcanic materials quenched from magmas (Klug and Cashman, 1996; Mueller et al., 2008; Colombier et al., 2017), which, taken together, provide a rich data resource for testing new, theoretical models. The scatter and range that can exist in permeability data for materials produced in nature and in the laboratory are prodigious due to the wide variety of microstructural geometries possible in magmas (e.g., vesicular, fractured, granular). Therefore, the most powerful and universal laws for how permeability varies with porosity have been built with a direct accounting for the microstructural origins (Martys et al., 1994; Wadsworth et al., 2016; Vasseur and Wadsworth, 2017; Giachetti et al., 2019).

Multiple discrete bubble nucleation events, continuous nucleation of bubbles, bubble coalescence, and differential bubble growth rates can all contribute to polydisperse bubble size distributions in magmas and pyroclasts (e.g., Blower et al., 2001). If the full size distribution of vesicles is constrained, then polydispersivity can be parameterized by a single metric (Torquato, 2013):

$$S = \frac{\langle R \rangle \langle R^2 \rangle}{\langle R^3 \rangle}, \quad (1)$$

where $\langle R^n \rangle$ is the n^{th} moment of the radius distribution with $\langle R \rangle$, $\langle R^2 \rangle$, and $\langle R^3 \rangle$ corresponding to the mean, variance, and skewness respectively. Collations of measured vesicle size distributions in erupted pyroclasts of pumice or scoria, and conversion of them to S via Equation 1, demonstrate that for all natural volcanic products, the vesicle sizes are highly polydisperse (Fig. 1). Despite this fact, no theoretical treatment of permeability exists for polydisperse bubble sizes that is valid from the lower limit of the percolation threshold (i.e., the point at which a cluster of bubbles first spans the system edge to edge) to the upper limit of foam at high porosity. In this contribution, we use a combination of collated published experimental data and novel numerical simulation results to test and validate a scaling for permeability that fully accounts for polydisperse bubble sizes. We show, in particular, that for the low values of S typical of natural systems, our new model predicts values of permeability that are many orders of magnitude different from those yielded by existing modeling approaches. We focus on the prograde path of bubble growth, in which the porosity is an increasing function of time.

METHODS

One highly effective approach to validating a model for magma permeability is to approximate a high-porosity bubbly magma as a system of overlapping spheres of the same porosity (Blower, 2001; Vasseur and Wadsworth, 2017). We adopt this geometric approach in the design of our numerical simulations. We place spheres of radius distribution $p(R)$ randomly in a periodic cube domain of edge length L (cf. Rintoul and Torquato, 1997; Vasseur and Wadsworth, 2017). We allow the spheres to overlap freely as we add them one by one. We define the spheres as the "bubble" phase, with porosity ϕ, and for this two-phase system, the inter-sphere phase represents the "groundmass" phase, with volume fraction $1 - \phi$. In contrast to previous models that have used monodisperse spheres, we here use a power-law size distribution such that the probability that a sphere has a radius between R and $R + dR$ is $p(R) = \alpha R^{-(\alpha+1)}$, where $\alpha > 3$ for three-dimensional (3-D) domains ($\alpha > 2$ for the two-dimensional [2-D] equivalent). We vary α across a wide range and then convert the resultant distributions of sizes into the polydispersivity S. For the probability density function $p(R)$ defined here, $\langle R^n \rangle = \alpha/(\alpha - n)$ for $n = 1$, 2, and 3. To illustrate our method, in Figure 2 we present rendered 3-D volumes in which we show only the fluid (non-solid) phase in a sub-volume.

For each new sphere we add to the domain, we use a Monte Carlo union-find algorithm to check if there is a cluster of connected spheres that span the domain from face to face (Newman and Ziff, 2001). Each new sphere increases the total number density by $1/L^3$ to N/L^3,

*E-mail: jeremie.vasseur@min.uni-muenchen.de

CITATION: Vasseur, J., Wadsworth, F.B., and Dingwell, D.B., 2020, Permeability of polydisperse magma foam: Geology, v. 48, p. 536–540, https://doi.org/10.1130/G47094.1

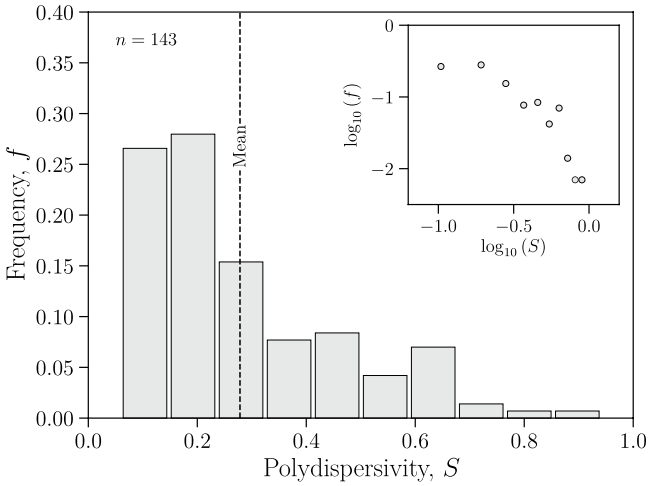

Figure 1. Polydispersivity of bubbles in natural pumice and scoria samples, cast as measured size distribution, taken from published data (Jutzeler et al., 2016, and references therein). For each measured distribution, we give the value of polydispersivity metric *S* and plot its resultant frequency distribution (each bin is expressed as a fraction of the total number of *S* values), showing that no natural sample can be approximated as monodisperse (*S* = 1) and that the mean value is *S* ≈ 0.28.

where N is the total number of spheres up to that point. As we increase N, there is a point beyond which the system has a connected phase across its length, which equates to a percolation porosity threshold ϕ_c. By repeating this process 10,000 times for each S and N, we can find the probability that $\phi \geq \phi_c$, which we term Π. The variation of Π with ϕ is sigmoidal, to which we fit the function: $\Pi = \{1 + \tanh[[\phi - \phi'_c(L)]/\Delta(L)]\}/2$. The fit parameters $\Delta(L)$ and $\phi'_c(L)$ are the width of the transition and the effective percolation threshold, respectively. In the GSA Data Repository[1], we plot these two parameters against one another, and following Sasidevan (2013), we can find the limiting ϕ_c as $\Delta \to 0$ (equivalent to an infinite domain size $L^3 \to \infty$). This represents constraint of the 3-D percolation threshold for overlapping spheres for any S.

We calibrate and check our method for constraining ϕ_c by performing the same analysis but in 2-D and comparing directly with the results of Sasidevan (2013), as well as by comparing our 3-D results in the monodisperse limit (for $S = 1$) with values reported previously (Rintoul and Torquato, 1997; Lorenz and Ziff, 2001; Vasseur and Wadsworth, 2017). In 2-D, $S = \langle R \rangle^2 / \langle R^2 \rangle$.

For each domain we generate for $\phi > \phi_c$, we use the LBflow code (Llewellin, 2010) to simulate fluid flow across the system through the sphere phase. We use input conditions for which the Reynolds (Re) and Mach (Ma) numbers are $\ll 1$, and for which Darcy's law applies at steady state. We impose a driving pressure gradient of $\nabla P = 0.01$ Pa·m^{-1}, and find $10^{-10} < \mathrm{Re} < 10^{-6}$ and $10^{-14} < \mathrm{Ma} < 10^{-9}$. We use a steady-state criterion such that the average speed across the entire lattice must not vary by more than a relative factor of 10^{-5} over 50 time steps, two times consecutively (Llewellin, 2010). The output is a simulation value of permeability k for each domain of a given ϕ and S. Example steady-state snapshots

[1]GSA Data Repository item 2020152, rigorous constraint of the percolation transition in 2-D and 3-D and the full reference list pertaining to Figure 1, is available online at http://www.geosociety.org/datarepository/2020/, or on request from editing@geosociety.org.

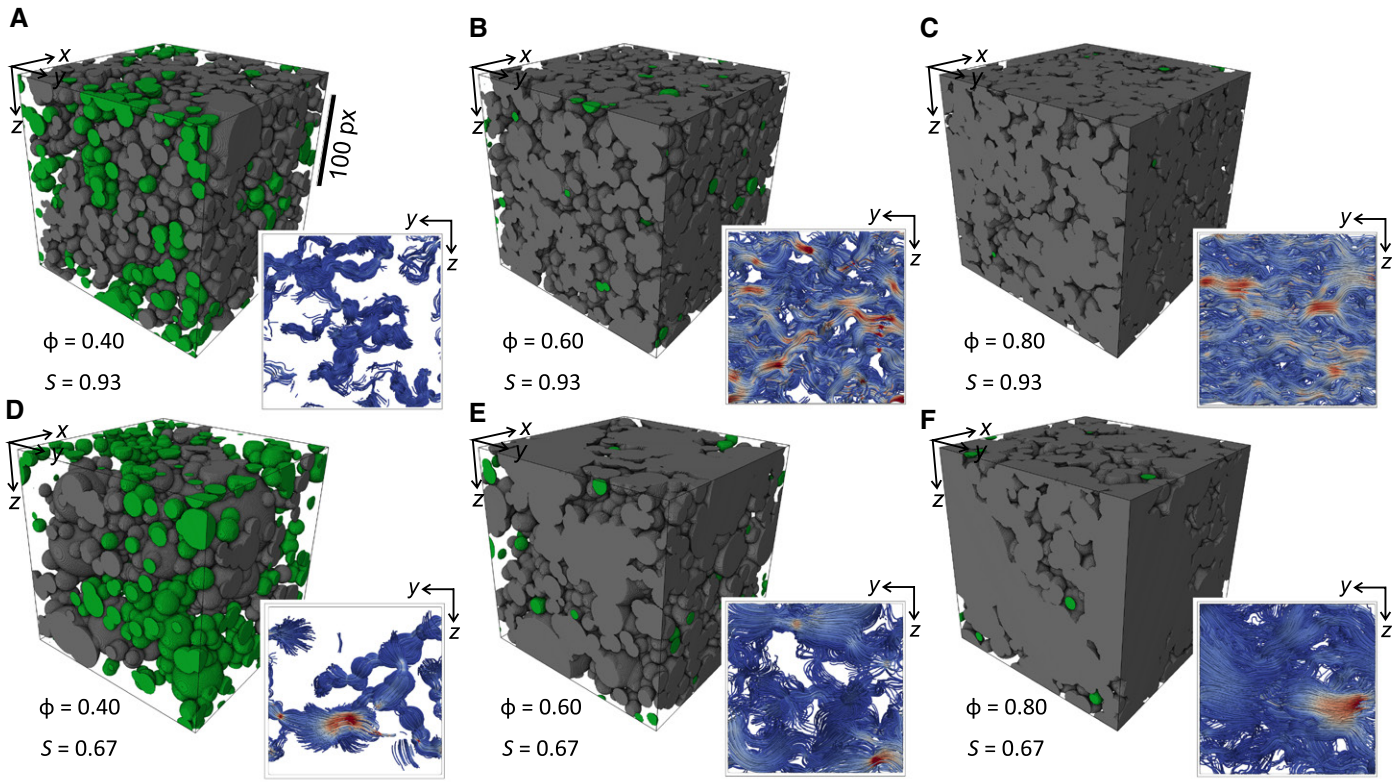

Figure 2. Rendered simulation volumes of polydisperse bubble networks at two different polydispersivity values (*S* = 0.93 and *S* = 0.67) for porosity ϕ = 0.4 (A, D), ϕ = 0.6 (B, E), and ϕ = 0.8 (D, F) (rendering produced using Avizo software, https://www.thermofisher.com/us/en/home/industrial/electron-microscopy/electron-microscopy-instruments-workflow-solutions/3d-visualization-analysis-software/avizo-materials-science.html). Green volumes represent bubbles isolated from edge-to-edge connections, while gray volumes represent fully connected bubble networks that can support permeable flow. Inset panels represent fluid-flow vector distribution collapsed onto a two-dimensional frame at steady state using LBflow code (Llewellin, 2010) from which permeability *k* is calculated. Blue-to-red gradient indicates low-to-high flow velocity (arbitrary scale for visual comparisons only). px—pixels.

of the fluid-flow vector field are shown in the insets to Figure 2. Taken together, these methods provide us with constraint of permeability and the percolation threshold as a function of bubble polydispersivity. Finally, we measure the specific surface area for each domain using a Lewiner marching cubes algorithm (Lewiner et al., 2003; Vasseur and Wadsworth, 2017).

RESULTS AND ANALYSIS

We use our method to predict the percolation threshold, and we find that it is dependent on the polydispersivity of bubble sizes. Our results show that in the monodisperse limit ($S = 1$), $\phi_c \approx 0.28934 \pm 0.00033$ (or equivalently $\phi_c \approx 0.67630 \pm 0.00001$ in the 2-D case). These values are within 0.08% of predictions given in previous work (Rintoul and Torquato, 1997; Lorenz and Ziff, 2001; Vasseur and Wadsworth, 2017). This result allows us to confidently explore polydisperse systems ($S < 1$). For $S < 1$, the percolation threshold diverges nonlinearly from the monodisperse limit toward very high values ($\phi_c \approx 1$) as the polydispersivity rises ($S \to 0$), which is shown in Figure 3A. This implies that polydisperse systems such as those found in natural pumice and scoria would be characterized by a higher percolation threshold than equivalent monodisperse systems, which verifies hypotheses made previously (Colombier et al., 2017). In the Data Repository, we collate these numerical results.

Our results also reveal that the permeability-porosity trend $k(\phi)$ is highly dependent on how polydisperse the growing bubble population is. To show this, we look for a simple, universal scaling law that can capture all of our results. The most successful universal scaling relationships for $k(\phi)$ for random heterogeneous media rely on the specific surface area of the pore network, s, and have the form $k \propto 1/s^2$ (Martys et al., 1994; Carman, 1997; Wadsworth et al., 2016). Torquato (2013) showed that for overlapping polydisperse sphere systems:

$$\bar{s} = s\frac{\langle R^3\rangle}{\langle R^2\rangle} = -3(1-\phi)\ln(1-\phi), \quad (2)$$

where $\bar{s} = sR$ in the monodisperse limit, and $\bar{s}$ is the normalized specific surface area. This relationship agrees well with our simulation result across all S (Fig. 3B). A scaling for $k(\phi)$ that relies on s has the advantage that the bubble size is not a direct input, which for polydisperse systems can be challenging to measure or constrain (Blower et al., 2001), and relies instead on bulk properties only. We use a simple form

$$k = \frac{1}{2Ss^2}\left(\phi - \phi_c\right)^b, \quad (3)$$

where b is the percolation exponent. For bubbly geometry relevant here, $b = 2.4$ has been predicted theoretically (Feng et al., 1987; where those authors use the term "inverted swiss cheese" to describe this geometry). We find excellent agreement between our measured k and the prediction of Equation 3 (Fig. 4). In Figure 4, we show the dimensionless result for a normalized permeability $\bar{k} = 2kSs^2$, as well as the dimensional results from our simulations.

Previous models for the permeability of systems with polydisperse bubble sizes do not include an account of ϕ_c (Costa, 2006). Here we demonstrate that ϕ_c is critical at high polydispersivity (Fig. 4A) and is clearly important in experimental data (Colombier et al., 2017). Much of the experimental data for magma or volcanic materials from which k and ϕ have been constrained are neither associated with a measured s, nor with the information required to predict s from the size distribution of pores, vesicles, or

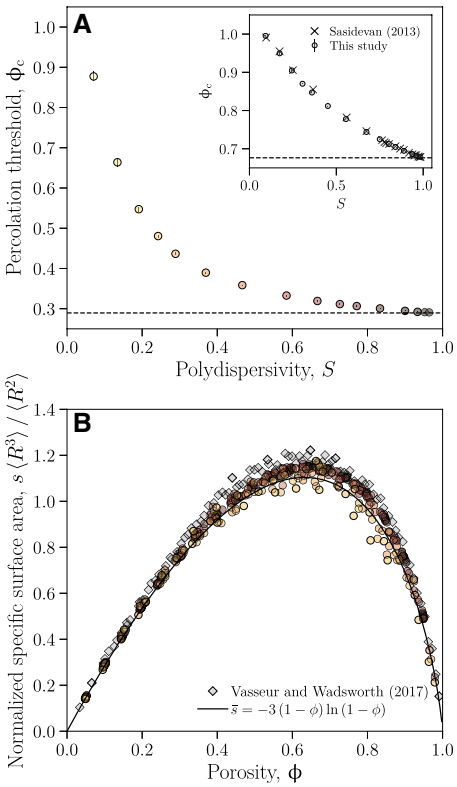

Figure 3. Results of our simulations showing dependence of percolation threshold on polydispersivity of bubble sizes in three-dimensional (inset: two-dimensional results) bubbly systems (A), and scaling for internal specific surface area of pore network for all polydispersivity (B). These parameters are used in the scaling of permeability (Fig. 4). Horizontal dashed line in A corresponds to monodisperse limit ($S = 1$).

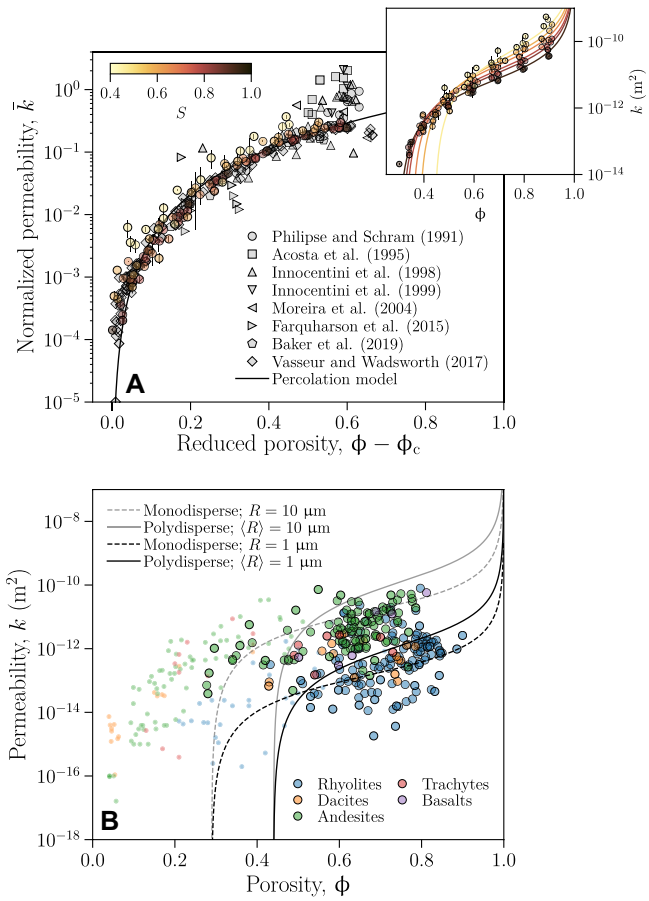

Figure 4. Scaled numerical results from our simulations of magma foam permeability between percolation porosity threshold ϕ_c and porosity $\phi \to 1$. (A) We cast permeability k in the universal normalized form $\bar{k} = 2kSs^2$ (S is polydispersivity, s is surface area of the pore network), for which the model form is $\bar{k} = (\phi - \phi_c)^{2.4}$. We compare this result against previously published data for which sufficient data exist, which includes permeability data for magmas collected *in situ* (Baker et al., 2019), volcanic rocks (Farquharson et al., 2015), analogous ceramic foams (Philipse and Schram, 1991; Acosta et al., 1995; Innocentini et al., 1998, 1999; Moreira et al., 2004), and for monodisperse sphere simulations (Vasseur and Wadsworth, 2017). Inset: Dimensional permeability-porosity relationships for our simulation results. (B) Our model (solid and dashed curves) solved for dimensional permeability k compared against a large compiled data set (Colombier et al., 2017, and references therein). R is radius, and $\langle R\rangle$ is radius distribution mean. Small data points are for products of effusive eruptions, while larger data points are for products of explosive eruptions.

bubbles (exceptions include Farquharson et al. [2015] and Baker et al. [2019]). Therefore, in order to further test our model against experimental data, we have chosen to scrutinize the family of open-celled foams in ceramic materials. Collating data for the permeability of ceramic solid open foams for which either s or $p(R)$ were measured (Philipse and Schram, 1991; Acosta et al., 1995; Innocentini et al., 1998, 1999; Moreira et al., 2004), we can apply our model directly. We find that our model accurately predicts experimental results in the foam limit without requiring empirical adjustment (Fig. 4A) to within approximately an order of magnitude at the highest porosities (with increasing accuracy for lower porosity). The ceramic foams used here have textures that are similar to those of, and are relevant for, high-porosity pyroclasts up to and including the reticulite open-foam limit (see Innocentini et al., 1998, their figure 2).

We also compare our model with a large compiled data set for the permeability of volcanic rocks (Colombier et al., 2017, and references therein). In Figure 4B, we focus on the permeability of rock products of explosive eruptions, and show that when our model is solved for the global mean $S = 0.28$ (Fig. 1), we predict that $\phi_c = 0.44$ (Fig. 3) and that the trends of $k(\phi)$ for reasonable mean vesicle sizes are consistent with the data. Therefore, we propose that our model captures the principal features of prograde degassing and the onset and evolution of the propensity for outgassing, as it is recorded in eruptive products here.

APPLICATIONS TO OUTGASSING THROUGH MAGMA FOAMS

The parameterization of permeability k given here is useful only for predicting outgassing rates in the low-Reynolds-number range where Darcy's law applies. However, outgassing through magma can have high velocity at shallow levels, such that the Reynolds number is unlikely to be low. Therefore, an additional constraint of the inertial contribution to flow through porous magma is required for our model to be of widest utility.

The average steady-state fluid velocity $\langle u \rangle$ that arises from a given pressure gradient ∇P can be predicted for any Reynolds number by the Forchheimer equation (Whitaker, 1996):

$$\nabla P = -\frac{\mu}{k}\langle u \rangle - \frac{\rho}{k_I}\langle u \rangle^2, \quad (4)$$

where μ and ρ are the fluid properties viscosity and density, respectively, and k_I is the inertial permeability. k_I can be predicted from k using a simple scaling $k_I = Ak^c$ where $A \approx 10^{10}$ and $c = 3/2$ (Zhou et al., 2019). This simple scaling coupled with Equations 1–4 and constitutive laws for the fluid properties provides a full quantitative description of fluid flow rates through porous magmas.

In our approach, we have made the simplifying assumption that a polydisperse bubbly magma can be approximated as a system of overlapping spheres. While this model approach is used widely (e.g., Blower, 2001; Vasseur and Wadsworth, 2017), the geometry imposed neglects the effects of bubble-bubble flattening and deformation prior to coalescence (Gonnermann et al., 2017) and the development of tube pumice (Dingwell et al., 2015), which have been observed and modeled. We note that textures that seem to record the capillary resistance of magma bubbles to coalescence may be one reason for the high percolation threshold invoked to explain magma bubbly permeability (Colombier et al., 2017; Giachetti et al., 2019). Similarly, it should be noted that the model neglects the effect of high crystal volume fractions, which can influence the permeability in a complex way (Lindoo et al., 2017). Nevertheless, we show quantitatively here that bubble polydispersivity also has a first-order effect on the percolation threshold (Fig. 3A) that has not been considered previously.

Coupling our model with Equation 4 provides a framework in which magma outgassing can be predicted. If this framework were embedded in a numerical model for magma expansion and compaction (e.g., Gonnermann et al., 2017), then the nonlinear feedback between gas pressure–driven magma porosity change and the local gas flow rates would be within our ability to predict.

CONCLUSIONS

Polydispersivity of bubble sizes in magma foams is crucial to predicting percolation threshold, pore surface areas, and permeability. Using numerical simulations, measurements on quenched volcanic materials, and constraints from analogous ceramic foams as a validation step, we provide a simple-to-use model for magma permeability. Using the Forchheimer equation, our model can be used to predict the local outgassing rates from open-celled magma foams in the shallow subsurface, of wide utility to gas monitoring efforts and to models that seek to predict the explosive potential of magma in various scenarios worldwide.

ACKNOWLEDGMENTS

We acknowledge support of the European Research Council (ERC) Advanced Grant on Experimental Access to Volcanic Eruptions: Driving Observational Potential (EAVESDROP, grant 834225). We thank the Leibniz Supercomputing Centre (LRZ) of the Bavarian Academy of Sciences and Humanities (Garching bei München, Germany) for computational support, as well as Jamie Farquharson, Thomas Shea, and one anonymous reviewer for constructive comments.

REFERENCES CITED

Acosta, F.A., Castillejos, E.A.H., Almanza, R.J.M., and Flores, V.A., 1995, Analysis of liquid flow through ceramic porous media used for molten metal filtration: Metallurgical and Materials Transactions: B, Process Metallurgy and Materials Processing Science, v. 26, p. 159–171, https://doi.org/10.1007/BF02648988.

Baker, D.R., Brun, F., Mancini, L., Fife, J.L., LaRue, A., O'Shaughnessy, C., Hill, R.J., and Polacci, M., 2019, The importance of pore throats in controlling the permeability of magmatic foams: Bulletin of Volcanology, v. 81, 54, https://doi.org/10.1007/s00445-019-1311-z.

Blower, J.D., 2001, Factors controlling permeability-porosity relationships in magma: Bulletin of Volcanology, v. 63, p. 497–504, https://doi.org/10.1007/s004450100172.

Blower, J.D., Keating, J.P., Mader, H.M., and Phillips, J.C., 2001, Inferring volcanic degassing processes from vesicle size distributions: Geophysical Research Letters, v. 28, p. 347–350, https://doi.org/10.1029/2000GL012188.

Carman, P.C., 1997, Fluid flow through granular beds: Process safety and environmental protection: Transactions of the Institution of Chemical Engineers: Part B, v. 75, p. S32–S48, https://doi.org/10.1016/S0263-8762(97)80003-2.

Cassidy, M., Manga, M., Cashman, K., and Bachmann, O., 2018, Controls on explosive-effusive volcanic eruption styles: Nature Communications, v. 9, 2839, https://doi.org/10.1038/s41467-018-05293-3.

Colombier, M., Wadsworth, F.B., Gurioli, L., Scheu, B., Kueppers, U., Di Muro, A., and Dingwell, D.B., 2017, The evolution of pore connectivity in volcanic rocks: Earth and Planetary Science Letters, v. 462, p. 99–109, https://doi.org/10.1016/j.epsl.2017.01.011.

Costa, A., 2006, Permeability-porosity relationship: A reexamination of the Kozeny-Carman equation based on a fractal pore-space geometry assumption: Geophysical Research Letters, v. 33, L02318, https://doi.org/10.1029/2005GL025134.

Degruyter, W., Bachmann, O., Burgisser, A., and Manga, M., 2012, The effects of outgassing on the transition between effusive and explosive silicic eruptions: Earth and Planetary Science Letters, v. 349, p. 161–170, https://doi.org/10.1016/j.epsl.2012.06.056.

Dingwell, D., Lavallée, Y., Hess, K., Flaws, A., Marti, J., Nichols, A.R.L., Gilg, H.A., and Schillinger, B.,2015, Eruptive shearing of tube pumice: Pure and simple: Solid Earth, v. 7, p. 1383–1393, https://doi.org/10.5194/se-7-1383-2016.

Farquharson, J., Heap, M.J., Varley, N.R., Baud, P., and Reuschlé, T., 2015, Permeability and porosity relationships of edifice-forming andesites: A combined field and laboratory study: Journal of Volcanology and Geothermal Research, v. 297, p. 52–68, https://doi.org/10.1016/j.jvolgeores.2015.03.016.

Feng, S., Halperin, B.I., and Sen, P.N., 1987, Transport properties of continuum systems near the percolation threshold: Physical Review B, v. 35, p. 197–214, https://doi.org/10.1103/PhysRevB.35.197.

Giachetti, T., Gonnermann, H.M., Gardner, J.E., Burgisser, A., Hajimirza, S., Earley, T.C., Truong, N., and Toledo, P., 2019, Bubble coalescence and percolation threshold in expanding rhyolitic magma: Geochemistry Geophysics Geosystems, v. 20, p. 1054–1074, doi: https://doi.org/10.1029/2018GC008006.

Gonnermann, H.M., Giachetti, T., Fliedner, C., Nguyen, C.T., Houghton, B.F., Crozier, J.A., and Carey, R.J., 2017, Permeability during magma expansion and compaction: Journal of Geophysical Research: Solid Earth, v. 122, p. 9825–9848, https://doi.org/10.1002/2017JB014783.

Innocentini, M.D.M., Sepulveda, P., Salvini, V.R., Pandolfelli, V.C., and Coury, J.R., 1998, Permeability and structure of cellular ceramics: A comparison between two preparation techniques: Journal of the American Ceramic Society, v. 81, p. 3349–3352, https://doi.org/10.1111/j.1151-2916.1998.tb02782.x.

Innocentini, M.D.M., Salvini, V.R., Macedo, A., and Pandolfelli, V.C., 1999, Prediction of ceramic foams permeability using Ergun's equation: Materials Research, v. 2, p. 283–289, https://doi.org/10.1590/S1516-14391999000400008.

Jutzeler, M., White, J.D.L., Proussevitch, A.A., and Gordee, S.M., 2016, Vesiculation and fragmentation history in a submarine scoria cone-forming eruption, an example from Nishiizu (Izu Peninsula, Japan): Bulletin of Volcanology, v. 78, 7, https://doi.org/10.1007/s00445-016-0999-2.

Klug, C., and Cashman, K.V., 1996, Permeability development in vesiculating magmas: Implications for fragmentation: Bulletin of Volcanology, v. 58, p. 87–100, https://doi.org/10.1007/s004450050128.

Lewiner, T., Lopes, H., Vieira, A.A.W., and Tavares, G., 2003, Efficient implementation of marching cubes' cases with topological guarantees: Journal of Graphics Tools, v. 8, p. 1–15, https://doi.org/10.1080/10867651.2003.10487582.

Lindoo, A., Larsen, J.F., Cashman, K.V., and Oppenheimer, J., 2017, Crystal controls on permeability development and degassing in basaltic andesite magma: Geology, v. 45, p. 831–834, https://doi.org/10.1130/G39157.1.

Llewellin, E.W., 2010, LBflow: An extensible lattice Boltzmann framework for the simulation of geophysical flows. Part II: Usage and validation: Computers & Geosciences, v. 36, p. 123–132, https://doi.org/10.1016/j.cageo.2009.08.003.

Lorenz, C.D., and Ziff, R.M., 2001, Precise determination of the critical percolation threshold for the three-dimensional "Swiss cheese" model using a growth algorithm: The Journal of Chemical Physics, v. 114, p. 3659–3661, https://doi.org/10.1063/1.1338506.

Martys, N.S., Torquato, S., and Bentz, D.P., 1994, Universal scaling of fluid permeability for sphere packings: Physical Review E, v. 50, p. 403–408, https://doi.org/10.1103/PhysRevE.50.403.

Moreira, E.A., Innocentini, M.D.M., and Coury, J.R., 2004, Permeability of ceramic foams to compressible and incompressible flow: Journal of the European Ceramic Society, v. 24, p. 3209–3218, https://doi.org/10.1016/j.jeurceramsoc.2003.11.014.

Mueller, S., Scheu, B., Spieler, O., and Dingwell, D.B., 2008, Permeability control on magma fragmentation: Geology, v. 36, p. 399–402, https://doi.org/10.1130/G24605A.1.

Newman, M.E.J., and Ziff, R.M., 2001, Fast Monte Carlo algorithm for site or bond percolation: Physical Review E, v. 64, p. 016706, https://doi.org/10.1103/PhysRevE.64.016706.

Philipse, A.P., and Schram, H.L., 1991, Non-Darcian airflow through ceramic foams: Journal of the American Ceramic Society, v. 74, p. 728–732, https://doi.org/10.1111/j.1151-2916.1991.tb06916.x.

Rintoul, M.D., and Torquato, S., 1997, Precise determination of the critical threshold and exponents in a three-dimensional continuum percolation model: Journal of Physics A: Mathematical and General, v. 30, L585, https://doi.org/10.1088/0305-4470/30/16/005.

Saar, M.O., and Manga, M., 1999, Permeability-porosity relationship in vesicular basalts: Geophysical Research Letters, v. 26, p. 111–114, https://doi.org/10.1029/1998GL900256.

Sasidevan, V., 2013, Continuum percolation of overlapping disks with a distribution of radii having a power-law tail: Physical Review E, v. 88, 022140, https://doi.org/10.1103/PhysRevE.88.022140.

Torquato, S., 2013, Random Heterogeneous Materials: Microstructure and Macroscopic Properties: New York, Springer Science & Business Media, 703 p.

Vasseur, J., and Wadsworth, F.B., 2017, Sphere models for pore geometry and fluid permeability in heterogeneous magmas: Bulletin of Volcanology, v. 79, p. 77, https://doi.org/10.1007/s00445-017-1165-1.

Wadsworth, F.B., Vasseur, J., Scheu, B., Kendrick, J.E., Lavallée, Y., and Dingwell, D.B., 2016, Universal scaling of fluid permeability during volcanic welding and sediment diagenesis: Geology, v. 44, p. 219–222, https://doi.org/10.1130/G37559.1.

Whitaker, S., 1996, The Forchheimer equation: A theoretical development: Transport in Porous Media, v. 25, p. 27–61, https://doi.org/10.1007/BF00141261.

Zhou, J.-Q., Chen, Y.-F., Wang, L., and Cardenas, M.B., 2019, Universal relationship between viscous and inertial permeability of geologic porous media: Geophysical Research Letters, v. 46, p. 1441–1448, https://doi.org/10.1029/2018GL081413.

Printed in USA